Scaling of Lift Reversal of Deformed Bubbles in Air-Water Systems

Hayashi, Kosuke
Hessenkemper, Hendrik
Lucas, Dirk
Legendre, Dominique
Tomiyama, Akio

(Citation)
International Journal of Multiphase Flow,142:103653

(Issue Date)
2021-09

(Resource Type)
journal article

(Version)
Accepted Manuscript

(URL)
https://hdl.handle.net/20.500.14094/90009447

Scaling of Lift Reversal of Deformed Bubbles in Air-Water Systems

Kosuke Hayashi[a], Hendrik Hessenkemper[b], Dirk Lucas[b],
Dominique Legendre[c], Akio Tomiyama[a,*]

[a] *Graduate School of Engineering, Kobe University, 1-1 Rokkodai Nada Kobe Hyogo, 657-8501 Japan*
[b] *Helmholtz-Zentrum Dresden-Rossendorf, Institute of Fluid Dynamics, Bautzner Landstraße 400, 01328 Dresden, Germany*
[c] *Institut de Mécanique des Fluides de Toulouse (IMFT) - Université de Toulouse, CNRS-INPT-UPS, 2 Allée du Professeur Camille Soula, 31400 Toulouse, France*

Abstract

Scaling of the lift reversal for a deformed bubble in the surface tension-inertial force dominant regime was discussed. Lift data of bubbles in water recently reported in literature were used. The negative lift component was well correlated in terms of the drag coefficient, which, in turn, implies that the vorticity produced at the bubble surface plays a key role in both drag and lift forces as is the case with the viscous force dominant regime. The scaling was confirmed to give good evaluations of the lift coefficients.

Keywords: lift force, lift reversal, negative lift, shape deformation

1. Introduction

Modeling the lift force acting on bubbles in liquids is of great importance to predict the distributions of volume fractions of each phase in bubbly flows. The lift coefficient, C_L, of bubbles has therefore been studied so far. It is well known that the lift coefficient of a spherical bubble is positive (positive lift) whatever the bubble Reynolds number is (Legendre and Magnaudet, 1998), while an ellipsoidal bubble experiences a negative lift force at large Reynolds numbers (Kariyasaki, 1987; Ervin and Tryggvason, 1997; Tomiyama, 1998; Tomiyama et al., 2002b; Adoua et al., 2009; Aoyama et al., 2017; Ziegenhein et al., 2018; Hessenkemper et al., 2020, 2021; Lee and Lee, 2020).

*Corresponding author
Email address: tomiyama@mech.kobe-u.ac.jp (Akio Tomiyama)

Tomiyama et al. (2002b) carried out experiments of single ellipsoidal bubbles in linear shear flows in the viscous force dominant regime (the μ regime) and proposed a C_L correlation using a modified Eötvös number, in which the bubble major axis is used for the characteristic length to account for the deformation effect on the lift reversal. Though several authors developed similar correlations to reproduce the lift reversal, such correlations using the modified Eötvös number only cannot account for the effects of the Morton number on the lift coefficient observed in experiments (Aoyama et al., 2017). Lee and Lee (2020) proposed a lift model for bubbles in the μ regime, which is expressed in terms of the bubble aspect ratio and the Ohnesorge number. Though their model can reproduce the lift reversal depending on the Morton number, the deviation from the experimental data increases with increasing shape deformation. We (Hayashi et al., 2020) proposed simple scaling for the lift reversal in the μ regime by connecting the negative lift with the vorticity produced at the bubble surface, which also plays a dominant role in the drag force (Legendre, 2007); in other words, the lift force is connected to the drag force via the vorticity (see Sec. 2 for detail).

With increasing the bubble size or with decreasing the liquid viscosity, a bubble is apt to be in the surface tension-inertial force dominant regime (the σ-i regime), e.g. the rise velocity of an air bubble larger than about 1.5 mm in stagnant water is to be governed by the Eötvös number, which is the ratio of the buoyancy to the surface tension force (Clift et al., 1978; Tomiyama et al., 1998). Since the bubble shape and motion exhibit complex oscillations it is not easy to obtain reliable data of the lift coefficient. Recently some studies reported novel measurement techniques for the lift coefficient of deformed bubbles with shape and path oscillations and provided lift databases (Hessenkemper et al., 2021; Lee and Lee, 2020), which would be of great use for scaling of the lift acting on deformed bubbles in the σ-i regime.

In this study, scaling of the lift reversal for deformed bubbles in linear shear flows in the surface tension-inertial force dominant regime is presented by making use of the available experimental databases of air bubbles in water.

2. Brief Review of C_L Models with Lift Reversal

The direction of the lateral migration of a bubble due to the shear-induced lift force depends on the sign of the lift coefficient C_L. The negative component of the lift is induced by the vorticity, ω, produced at the bubble surface (Adoua et al., 2009), which increases with increasing the aspect ratio, χ ($= d_H/d_V$), of an ellipsoidal bubble, where d_H and d_V are the major and minor axes of the bubble. Legendre (2007) pointed out that the drag is proportional to the vorticity, and the viscous contribution appears in the lift of a spherical bubble in the form of Re^{-1}, being similar to the drag (Legendre and Magnaudet, 1998), where Re is the bubble Reynolds number defined by

$$Re = \frac{\rho_L V_R d}{\mu_L} \tag{1}$$

where ρ_L is the liquid density, V_R the bubble relative velocity, d the sphere-volume-equivalent bubble diameter, and μ_L the liquid viscosity. Therefore the drag and the negative lift in the μ regime are connected as follows (Hayashi et al., 2020):

$$C_L = C_L^{S\infty} - G_r(\chi, Re) C_D \tag{2}$$

where C_D is the drag coefficient, $G_r(\chi, Re)$ a function of χ and Re, and $C_L^{S\infty}$ ($= 1/2$) the lift coefficient of a spherical bubble in an inviscid shear flow (Auton, 1987). We obtained the following expression of C_L, which is explicitly relating with the vorticity:

$$C_L = C_L^{S\infty} - \gamma_r \frac{16}{Re} \phi(\chi, Re) \omega_{\max}^{*\infty}(\chi) \tag{3}$$

where $\gamma_r = 0.078$, $\omega_{\max}^{*\infty}$ is the dimensionless maximum vorticity in the infinite Reynolds number limit (Magnaudet and Mougin, 2007)

$$\omega_{\max}^{*\infty}(\chi) = \frac{2\chi^{5/3}(\chi^2-1)^{3/2}}{\chi^2 \sec^{-1}\chi - (\chi^2-1)^{1/2}} \tag{4}$$

and $\phi(\chi, Re)$ ($= 0.25\chi^{1.9} Re^{0.32}$) is the deformation-inertia factor in the drag correlation proposed by Chen et al. (2019). Equation (3) expresses well the behavior of C_L of a deformed bubble. We, therefore, proposed the following empirical correlation by connecting

the negative lift and C_L of spherical bubbles to cover low and intermediate Re:

$$C_L = C_L^S - \frac{g(M)(\chi - 1)^{h(M)}}{Re} \tag{5}$$

where

$$g(M) = a \exp(-bM^c) \tag{6}$$

$$h(M) = p \exp(-qM^r) \tag{7}$$

and M is the Morton number defined by

$$M = \frac{\mu_L^4 \Delta\rho g}{\rho_L^2 \sigma^3} \tag{8}$$

where $\Delta\rho$ is the density difference between the two phases, g the acceleration of gravity, and σ the surface tension. The constants in Eqs. (6) and (7) are as follows: $a = 500$, $b = 6.0$, $c = 0.0735$, $p = 3.46$, $q = 5.4$ and $r = 0.191$. The C_L^S is the lift coefficient of a spherical bubble (Legendre and Magnaudet, 1998):

$$C_L^S = ([C_L^{SL}]^2 + [C_L^{SH}]^2)^{1/2} \tag{9}$$

where the lift coefficients of a low Reynolds number bubble, C_L^{SL}, and a high Reynolds number bubble, C_L^{SH}, are defined by

$$C_L^{SL} = \frac{6}{\pi^2} \frac{2.255}{\sqrt{SrRe}\,[1 + 0.2Re/Sr]^{3/2}} \tag{10}$$

$$C_L^{SH} = \frac{1}{2}\left(\frac{1 + 16/Re}{1 + 29/Re}\right) \tag{11}$$

Here the dimensionless shear rate, Sr, is defined by

$$Sr = \frac{\Omega d}{V_R} \tag{12}$$

where Ω is the vorticity of a linear shear flow. Equation (5) agrees well with the experimental data of C_L in the μ regime (Aoyama et al., 2017). Lee and Lee (2020) also accounted for

the effects of ω on C_L in their lift modeling and proposed the following C_L correlation for bubbles in the μ regime:

$$C_L = \begin{cases} C_L^{S\infty} - 2.8\chi^{2.2}Oh & \text{for } Re > 4 \\ \max\left[C_L^{SL}, C_L^{S\infty} - 2.8\chi^{2.2}Oh\right] & \text{for } Re \leq 4 \end{cases} \tag{13}$$

where Oh is the Ohnesorge number defined by

$$Oh = \frac{\mu_L}{\sqrt{\rho_L \sigma d}} \tag{14}$$

which can be expressed as $Oh = \sqrt{Ca/Re}$, where Ca is the capillary number defined by $Ca = \mu_L V_R/\sigma$. The lift reversal is reproduced by the correlation and good agreement with Aoyama's data can be obtained at large M numbers, while the deviation from the data increases as M decreases. This would be due to the use of the relation, $\omega^*_{\max} = \chi$, which is valid only for low Reynolds number bubbles (Legendre, 2007).

Bubbles in the μ regime rectilinearly rise in a stagnant liquid without shape oscillation. With increasing bubble diameter and/or decreasing the liquid viscosity, the motion of a bubble becomes unstable and the bubble path becomes zigzagging or spiraling. Larger bubbles exhibit wobbling motion and the path oscillation is more complicated due to capillary waves formed at the bubble surface. A difficulty in forming a fully-developed linear shear flow of a low viscosity liquid in a lab scale apparatus and a stochastic nature of the fluctuating bubble path make it difficult to obtain reliable C_L databases for bubbles in the σ-i regime. Ziegenhein et al. (2018) developed a novel technique for lift force measurement in the σ-i regime of an air-water system, which makes use of a bubble plume to form a linear shear field about a single bubble. The lift reversal in this low viscosity system takes place at $Re \approx 1000$, which corresponds to $Eo_H \approx 5$, where Eo_H is the Eötvös number using d_H for the characteristic length (Tomiyama et al., 2002b):

$$Eo_H = \frac{\Delta\rho g d_H^2}{\sigma} \tag{15}$$

Hessenkemper et al. (2020) applied the measurement technique to study effects of sodium chloride on C_L and more data of C_L were accumulated in Hessenkemper et al. (2021) for purified and slightly impure systems.

Lee and Lee (2020) modeled the lift acting on a deformed bubble with a sinusoidally oscillating path in an air-water system based on the estimation of the orders of the lift induced by double-threaded vortex filaments formed behind a bubble (de Vries et al., 2002) and of the decay of the vortex filaments due to the viscosity (Saffman, 1992). The wake-induced negative lift was expressed in terms of the characteristic time t_c for the diffusion of vortex filaments detaching from a bubble, the characteristic length l of the detached vortex filaments, the amplitude X of the zigzagging path, and the dimensionless vorticity $\omega^*_{\max}$ at the bubble equator. The t_c was estimated as $t_c = 1/f_{(2,0)}$ (Veldhuis et al., 2008), where $f_{(2,0)}$ is the shape oscillation frequency (Lunde and Perkins, 1998). The l was assumed to be $l = d_H$, and X was estimated as $d_H/2$ from their experiments, which is much smaller than some measured data in stagnant water (Tomiyama et al., 2002a). Equation (4) was used for $\omega^*_{\max}$. By using these expressions for t_c, l, X and $\omega^*_{\max}$, Lee and Lee (2020) obtained the following correlation:

$$C_L = C_L^{S\infty} - \frac{12\pi}{2^{-1/4}} \frac{\chi^{4/3}(\chi^2+1)^{3/4}(\chi^2-1)^{3/2}}{\chi^2 \sec^{-1}\chi - (\chi^2-1)^{1/2}} Oh \tag{16}$$

The constant in the denominator is given as $2^{3/4}$ in the original paper, however it should read $2^{-1/4}$. Lee and Lee (2020) also carried out experiments on C_L of bubbles in linear shear flows in water, in which d ranged from 2 to 20 mm and Re ranged from 440 to 7180. The model was compared with the experimental data and was confirmed to express the trend of C_L with increasing Eo_H. Although their model reproduces the decay of C_L due to the negative lift component, the deviation between the model and the data is apt to be large except around the critical bubble diameter for the onset of lift reversal as shown in Sec. 4.1.

3. Datasets

A dataset of 19 data points for bubbles in purified water presented in Hessenkemper et al. (2021) is used in the following data analysis. Lee and Lee (2020) tabulated their data (11 data points) of bubbles in filtered water. They provided two sets of C_L data: C_L were evaluated based on the force balance between the drag, lift and buoyancy in one of them, while in the other set they evaluated C_L by additionally accounting for the accelerated motion of a bubble. We use the former in this study since some data in the latter largely scatter and exhibit standard deviations much larger than the former. The ranges of relevant dimensionless groups in the experimental data are summarized in Table 1. Both datasets cover the positive and negative lift regimes. The order of Re ranges from O(10^2) to O(10^3), and the Re range of the Lee data is wider than that of Hessenkemper's data. The dimensionless shear rate, Sr, is much smaller than unity, and therefore, the lift discussed here is for bubbles under weak shear flows. The Eötvös number, Eo, and Weber number, We, in the table are defined by

$$Eo = \frac{\Delta\rho g d^2}{\sigma} \tag{17}$$

$$We = \frac{\rho_L V_R^2 d}{\sigma} \tag{18}$$

4. Discussion

4.1. Data analysis

Figure 1 shows a *Re*-*Eo* map (Tomiyama et al., 1998) and the dataset are plotted on it. The dashed line represents the transition from the Re-controlling regime (μ regime) to the Eo-controlling regime (σ-i regime). Most of the data in Aoyama et al. (2017) lie below the transition line and their bubbles rose rectilinearly with no path/shape oscillation, and therefore, their data were in the μ regime. On the other hand, the data of Hessenkemper et al. (2021) and Lee and Lee (2020) are in the Eo-controlling regime and bubbles showed fluctuating paths. Their data were therefore in the σ-i regime.

Table 1: Ranges of dimensionless groups in dataset (*:Hessenkemper et al. (2021), †: Lee and Lee (2020))

Source	H*	L†
Number of data	19	11
Water	purified	filtered
$\log M$	-10.58	-10.84
Re	680 - 1470	440 - 7170
Eo	0.70 - 5.6	0.63 - 55
We	2.9 - 4.7	0.92 - 26
Sr	O(10^{-2})	O(10^{-3}) - O(10^{-2})
χ	1.96 - 2.1	1.13 - 3.26
C_D	0.32 - 1.58	0.919 - 2.78
C_L	-0.34 - 0.38	-2.74 - 0.57

The C_D in the dataset are shown in Fig. 2. The solid line represents the following drag correlation applicable to the σ-i regime (Tomiyama et al., 1998):

$$C_D = \frac{8}{3}\frac{Eo}{Eo+4} \tag{19}$$

The data of Hessenkemper et al. (2021) agree well with the correlation. Though the dependence of C_D on Eo is the same in Lee's data, they are systematically larger than Eq. (19) in the whole Eo range. Though the liquid flows in their experiments exhibited some turbulence fluctuations, the C_D data in the linear shear flows agreed well with their C_D data in stagnant water. The turbulence effect is therefore not the cause of the large C_D of Lee's data. See Appendix A for brief discussion on the turbulence effect on the drag and the lift. The other possibility is unintentional contamination of water, which increases C_D due to Marangoni effect.

Bubbles in the air-water experiments showed wobbling and/or meandering motion. The longest axis of a bubble shape projected on the front-camera view was therefore used as d_H. The aspect ratio data of Hessenkemper et al. (2021) are shown in Fig. 3 with the data of Sugihara et al. (2007) for bubbles in ultra purified water in the μ regime. The χ increases

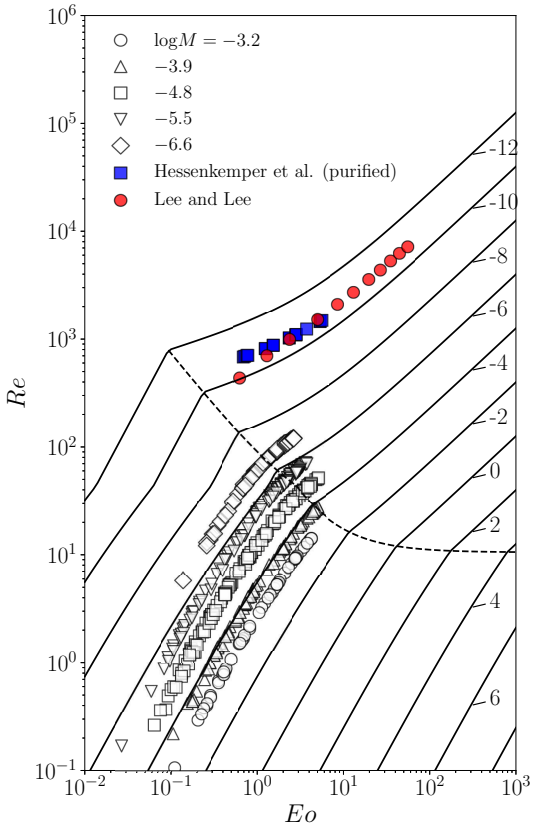

Figure 1: Dataset on *Re*-*Eo* plane (Tomiyama et al., 1998). Labels represent log$M$.

with increasing Eo in the μ regime and reaches about $\chi = 2$ at $Eo = 0.5$. Then χ also increases with Eo in the σ-i regime, whereas the increasing rate is drastically smaller than in the μ regime. Sugihara et al. (2007) fitted the functional form proposed by Wellek et al. (1966)

$$\chi = 1 + aEo^b \tag{20}$$

to their data and obtained $a = 6.5$ and $b = 1.925$. Fitting this functional form to the Hessenkemper data gives much smaller values for the coefficients, i.e. $a = 0.94$ and $b = 0.0875$, as shown in the figure (solid line). The χ in Lee's data also show monotonous increase and Lee and Lee (2020) proposed $a = 0.21$ and $b = 0.58$ as represented by the dotted line, which agrees well with the data.

The χ of Hessenkemper et al. (2021) seems to be continous with those in the μ regime. On

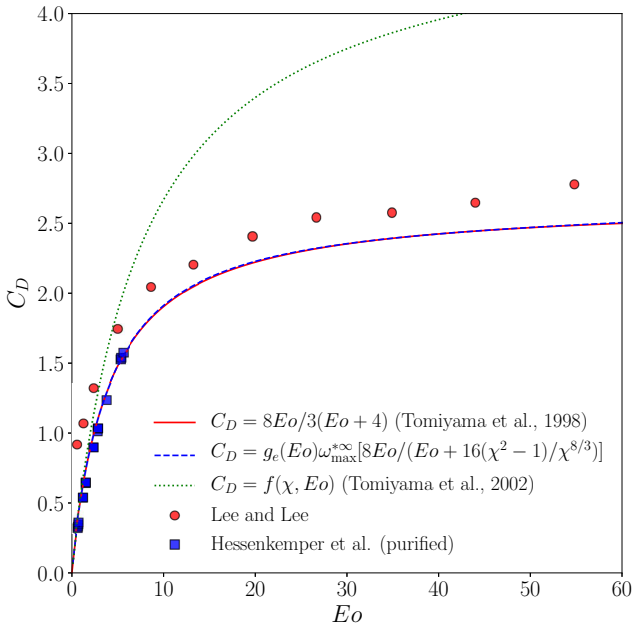

Figure 2: Drag coefficient C_D. Eqs. (24) and (19) are used for χ in $C_D(\chi, Eo)$. The solid and dashed lines are overlapped.

the other hand, Lee's data show much weaker shape deformation, e.g. $\chi \approx 1.1$ at $Eo = 0.63$. This value is close to that of a bubble in a contaminated system rather than a clean system (Clift et al., 1978). In addition, the following shape correlation for contaminated bubbles proposed by Fan and Tsuchiya (1990) agrees well with Lee's data.

$$\chi = \begin{cases} 1 & \text{for } Ta < 1 \\ [0.81 + 0.20\tanh(2.0(0.80 - \log Ta))]^{-3} & \text{for } 1 \le Ta \le 40 \\ 4.17 & \text{for } Ta > 40 \end{cases} \tag{21}$$

where Ta is the Tadaki number defined by

$$Ta = ReM^{0.23} \tag{22}$$

Thus bubbles in Lee's data must have been contaminated.

It would be worth discussing the dependence of χ on We. Figure 4 shows the data of Hessenkemper et al. and Sugihara et al. on the χ-We plane. Being similar to the trend on the χ-Eo plane, those data seem continuous and the change in the dependence of χ on We

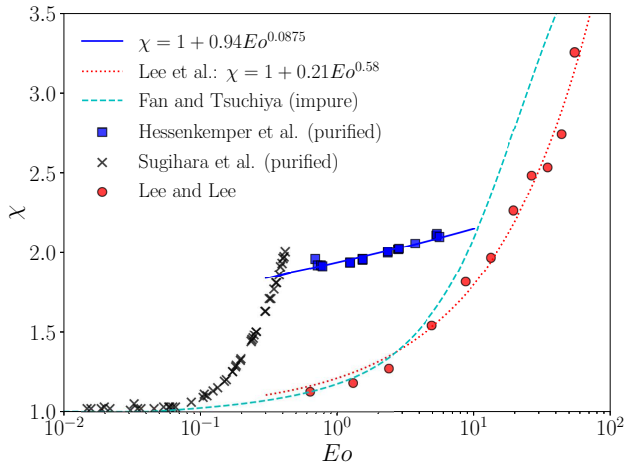

Figure 3: Bubble aspect ratio χ.

from the μ regime to the σ-i regime is obvious. The critical We for the regime transition is about 3, which is consistent with the experimental result of Duineveld (1995). The dashed line represents the following empirical correlation proposed by Sugihara et al.:

$$\chi = 1 + \frac{9}{64}We + \frac{0.04We^2}{\sqrt{3.7 - We}} \tag{23}$$

This correlation developed for the μ regime rapidly increases for We larger than 3 due to the factor of $(3.7 - We)^{-1/2}$. The solid line is a fitting equation for Hessenkemper's data in terms of We:

$$\chi = 1 + cWe^d \tag{24}$$

where $c = 0.62$ and $d = 0.376$. Experimental data of Aybers and Tapucu (1969) and Duineveld (1995) obtained for bubbles in filtered and ultra pure water, respectively, are also shown in the figure. Duineveld's data are similar to Sugihara's data and Duineveld reported $We = 3.3$ for the onset of the bubble path instability. Aybers' data seem to lie on the same curve with Duineveld's data even for $We > 3.3$ and they are well expressed by the following correlation developed for a wide range of M (dash-dotted line) (Legendre et al., 2012):

$$\chi = \frac{1}{1 - \frac{9}{64}\frac{We}{1+0.2M^{0.1}We}} \tag{25}$$

In Aybers and Tapucu (1969), bubbles larger than 1.34 mm showed path oscillations, whereas they initially rose along rectilinear paths up to certain elevations. It should be noted that

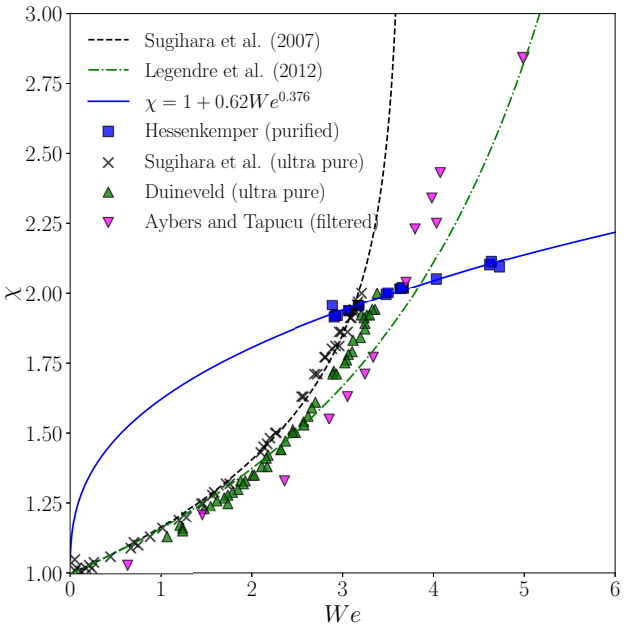

Figure 4: Bubble aspect ratio plotted against We.

the shape data were evaluated within the rectilinear path range. This explains why their data follow the same curve as in the μ regime even for $We > 3$.

The C_L data are plotted against Oh in Fig. 5 and compared with Lee's model, Eq. (16). The model qualitatively represents the decay of C_L due to the negative lift. However the deviation tends to be large especially in the negative C_L region, and the negative lift component in the positive C_L region is overestimated, e.g. the C_L data at $Oh = 0.00218$ is close to 0.5 under moderate deformation ($\chi = 1.1$) while the model gives a smaller value, $C_L = 0.138$, due to a strong negative lift. As for the condition for the lift reversal, the bubble diameter corresponding to $C_L = 0$ in Lee's data is about 6 mm ($Oh = 0.0013$) and Lee's model predicts $d = 6.7$ mm ($Oh = 0.00124$). The critical diameter, $d = 4.5$ mm for $Oh = 0.0017$, in the clean system of Hessenkemper et al. (2021) is smaller compared with Lee's data.

Figure 6 shows the C_L data plotted against Re. The C_L data of Aoyama et al. (2017) for the μ regime are also plotted for reference. The range of M in Aoyama et al. (2017) is $-6.6 \leq \log M \leq -3.2$. Aoyama's data cover from low Re to intermediate Re, i.e. $0.1 <$

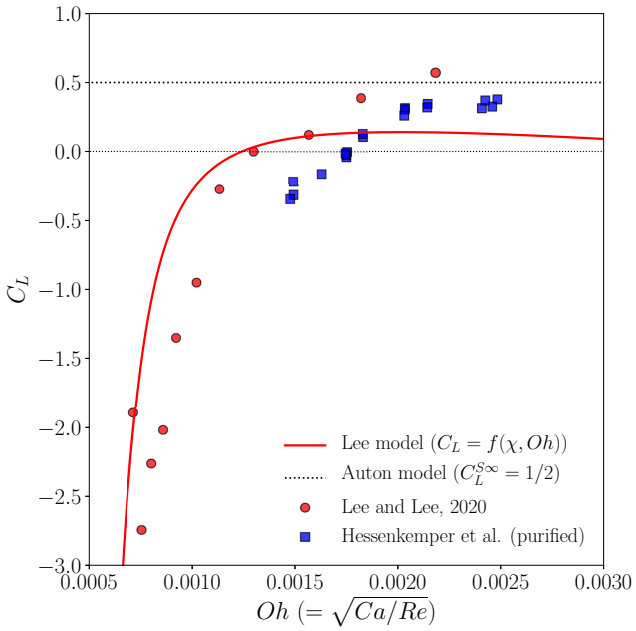

Figure 5: Lift coefficient, C_L, plotted against Ohnesorge number. The solid line is Eq. (16) and the aspect ratio in Eq. (16) is evaluated using $\chi = 1 + 0.21Eo^{0.58}$.

$Re < 120$, in which the bubble shape changes from spherical to ellipsoidal as Re increases. The Re in the air-water system are much higher than Aoyama's data. The air-water data show that the increase in Re decreases C_L and C_L becomes negative at Re larger than a certain critical value as in the μ regime. Although the critical Re in the air-water systems show some differences, it lies within $1000 < Re < 1600$. It seems that the upperbound of C_L of ellipsoidal bubbles can be well expressed by the Legendre-Magnaudet correlation, Eq. (9) for spherical bubbles, which approaches $C_L^{S\infty} = 1/2$ at $Re \sim 1000$. In fact, for fixed non-deformable ellipsoidal bubbles, Adoua et al. (2009) found a larger upperbound of C_L, i.e. $C_L^{\infty} = 0.5 + 0.612(\chi - 1)$, and, for example, $C_L \approx 1.0$ at $Re = 1000$ and $\chi = 2.0$ in their numerical simulation. In contrast to Adoua's numerical simulations, bubbles in the experiments are not exact ellipsoid, free to move, and possible to incline from the streamwise direction, which may decrease C_L and consequently restrict the maximum possible C_L.

In both air-water data, C_L monotonously decreases with increasing Re and χ as in the μ regime. As shown in the dotted line in the figure, the empirical correlation, Eq. (5), can

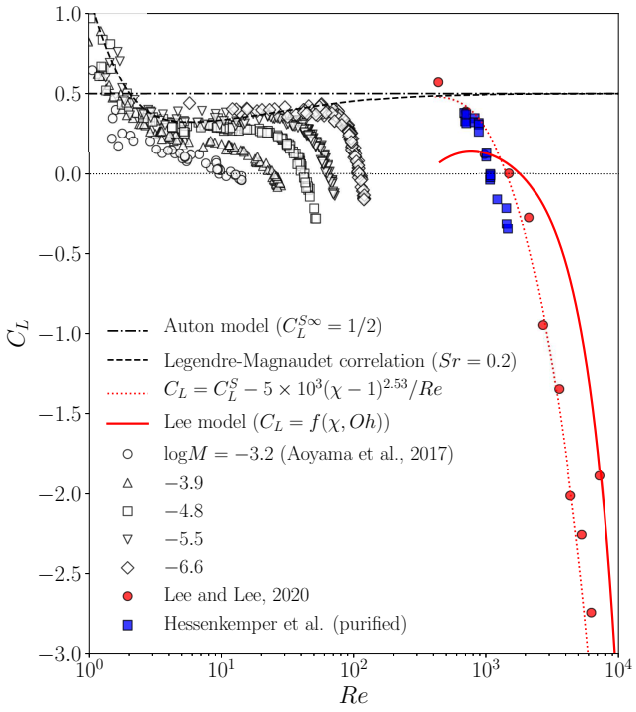

Figure 6: Lift coefficient, C_L, plotted against Reynolds number. The χ and Re are evaluated by using the χ correlation, Eq. (20), with Lee's coefficients and the drag correlation, Eq. (19), respectively, to draw the correlation curve for Lee's data (dotted line).

be used to express the data of the contaminated system in Lee and Lee (2020) by tuning the coefficients in the correlation for the data, i.e. $C_L = C_L^S - 5 \times 10^3(\chi - 1)^{2.53}/Re$, where the power 2.53 is the same as that for log$M = -6.6$ in Eq. (7), while the coefficient 5×10^3 is much larger than that of the original correlation. This trend is consistent with the fact that the interfacial vorticity is increased at an interface partially immobilized due to contamination. On the other hand, a much larger value is required for the power of $\chi - 1$ to fit the functional form to the data of clean bubbles of Hessenkemper et al. (2021). This can be clearly seen in Fig. 7, where the vertical and horizontal axes are $(C_L^S - C_L)Re$ and $\chi - 1$, respectively, and therefore, the slope of the data represents $h(M)$ in Eq. (5). Hessenkemper's data show steep increase and the trend is different from the data for the μ regime. This is due to very small change in χ even with a considerable change in Re by a factor of about 2.

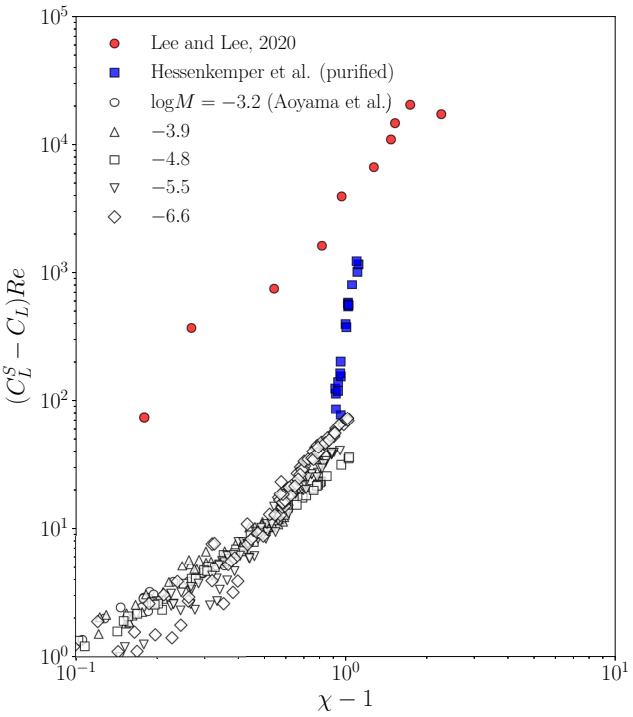

Figure 7: Difference between C_L and the correlation, C_L^S, for spherical bubbles (Legendre and Magnaudet, 1998).

4.2. C_L Scaling in the Surface Tension-Inertial Force Dominant Regime

In this section, we will make an attempt to find an explicit relation between the vorticity produced at the bubble surface and both the drag and lift forces as we conducted for the μ regime in our previous study (Hayashi et al., 2020) to obtain appropriate scaling of C_L in the σ-i regime. The clean bubble data of Hessenkemper et al. (2021) are used for this purpose.

Let us consider how $\omega^*_{\max}$ appears in C_D of the σ-i regime. Tomiyama et al. (2002a) derived the following terminal velocity model for ellipsoidal bubbles in stagnant liquid:

$$V_T = F(E)\sqrt{\frac{8\sigma}{\rho_L d}E^{4/3} + \frac{\Delta\rho g d}{2\rho_L}\frac{E^{2/3}}{1-E^2}} \tag{26}$$

where $E = 1/\chi$, V_T is the terminal velocity of a bubble, and

$$F(E) = \frac{\sin^{-1}\sqrt{1-E^2} - E\sqrt{1-E^2}}{1-E^2} \tag{27}$$

The drag coefficient for this velocity model is given by

$$C_D = \frac{4}{3}\frac{2Eo(1-E^2)}{16E^{4/3}(1-E^2)+EoE^{2/3}}F(E)^{-2} \tag{28}$$

Rewriting this by replacing E with χ and using $\omega_{\max}^{*\infty}$ in the infinite Re limit, Eq. (4), yield

$$C_D(\chi, Eo) = f_e(\chi)\omega_{\max}^{*\infty}\left[\frac{8}{3}\frac{Eo}{Eo+16(\chi^2-1)/\chi^{8/3}}\right] \tag{29}$$

where

$$f_e(\chi) = \frac{(\chi^2-1)^{3/2}}{2\chi^3[\chi^2\sec^{-1}\chi-(\chi^2-1)^{1/2}]} \tag{30}$$

The factor in the square brackets of Eq. (29) is equivalent to $C_D = 8Eo/3(Eo+4)$ when $\chi = 1.18$. The χ in Eq. (29) can be evaluated by making use of Eqs. (24) and (19). As shown in Fig. 2 (the dotted line), this model agrees well with Hessenkemper's data at small Eo but overestimates C_D in the large Eo range since it is for perfect spheroidal bubbles without wobbling motion. The following simple modification however gives good evaluations of C_D for the whole Eo range of the data as shown in Fig. 2 by the dashed line:

$$C_D(\chi, Eo) = g_e(Eo)\omega_{\max}^{*\infty}\left[\frac{8}{3}\frac{Eo}{Eo+16(\chi^2-1)/\chi^{8/3}}\right] \tag{31}$$

where

$$g_e(Eo) = \frac{0.177}{(1+0.33Eo)^{0.65}} \tag{32}$$

We have thus obtained the expression of C_D in the σ-i regime connected with the vorticity. Although the above modification is made for the present system of $\log M = -10.58$, there might be a possibility that the modification is applicable to lower Morton number systems as follows. As seen in the shape correlation, Eq. (25), χ can be written as a function of We and M. Hence $f_e(\chi) = f_e(We, M)$. The $f_e(We, M)$ can also be written as $f_e(Eo, M)$ by using the force balance between the drag and the buoyancy $C_D = 4/3Fr^2$, the relation $We = Fr^2Eo$ by definition and Eq. (19), where $Fr = V_R/\sqrt{\Delta\rho gd/\rho_L}$ is the Froude number. Hence the function, $g_e(Eo)$, of Eo only should be regarded as a modification of $f_e(Eo, M)$ for the specific Morton number. However the factor for the Morton number effect, $K(M) = 0.2M^{0.1}$, in Eq. (25) at $\log M = -10.58$ is only 0.017 and $K(M)$ decreases with decreasing M. Hence

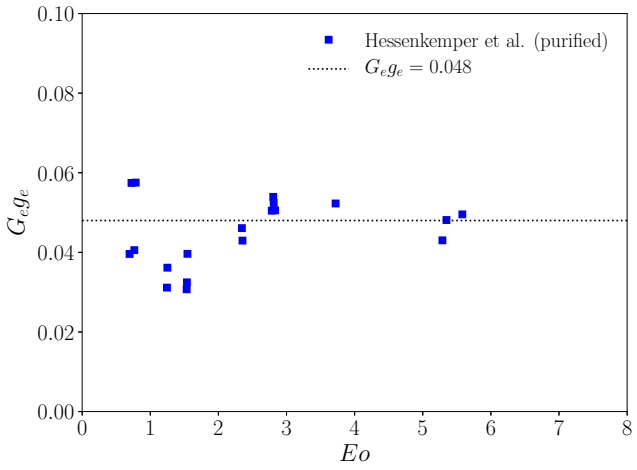

Figure 8: Product of the factor $G_e g_e$ ($= (C_L^S - C_L)/[\omega_{\max}^{*\infty}(8Eo)/3(Eo + 16(\chi^2-1)/\chi^{8/3})]$) for the connection between C_D and the negative lift.

the Morton number effect on χ is very weak for $\log M \leq -10.58$ and $g_e(Eo)$ is expected to be applicable within this M range.

We assume that the negative lift is also connected with the vorticity via the drag as in the μ regime:

$$C_L = C_L^S(Re, Sr) - G_e(\chi, Eo) C_D(\chi, Eo) \tag{33}$$

where G_e is a function of χ and Eo. Substituting Eq. (31) into this equation yields

$$C_L = C_L^S(Re, Sr) - G_e(\chi, Eo) g_e(Eo) \omega_{\max}^{*\infty}(\chi) \left[\frac{8}{3} \frac{Eo}{Eo + 16(\chi^2 - 1)/\chi^{8/3}} \right] \tag{34}$$

Figure 8 shows G_e evaluated from the data. Although some scatter appears at small Eo, the G_e data show a constant value for the product $G_e(\chi, Eo) g_e(Eo)$. Hence

$$C_L = C_L^S(Re, Sr) - \gamma_e \omega_{\max}^{*\infty}(\chi) \left[\frac{8}{3} \frac{Eo}{Eo + 16(\chi^2 - 1)/\chi^{8/3}} \right] \tag{35}$$

where $\gamma_e = 0.048$.

A comparison between the data and Eq. (35) (solid lines) on the C_L-Eo plane is shown in Fig. 9(a), where Eqs. (19) and (24) were used to calculate Re and χ, respectively. Good agreement is obtained between Eq. (35) and Hessenkemper's data. The evaluations of Eq. (35) are not so different from Lee's data at large Eo. The following empirical correlation

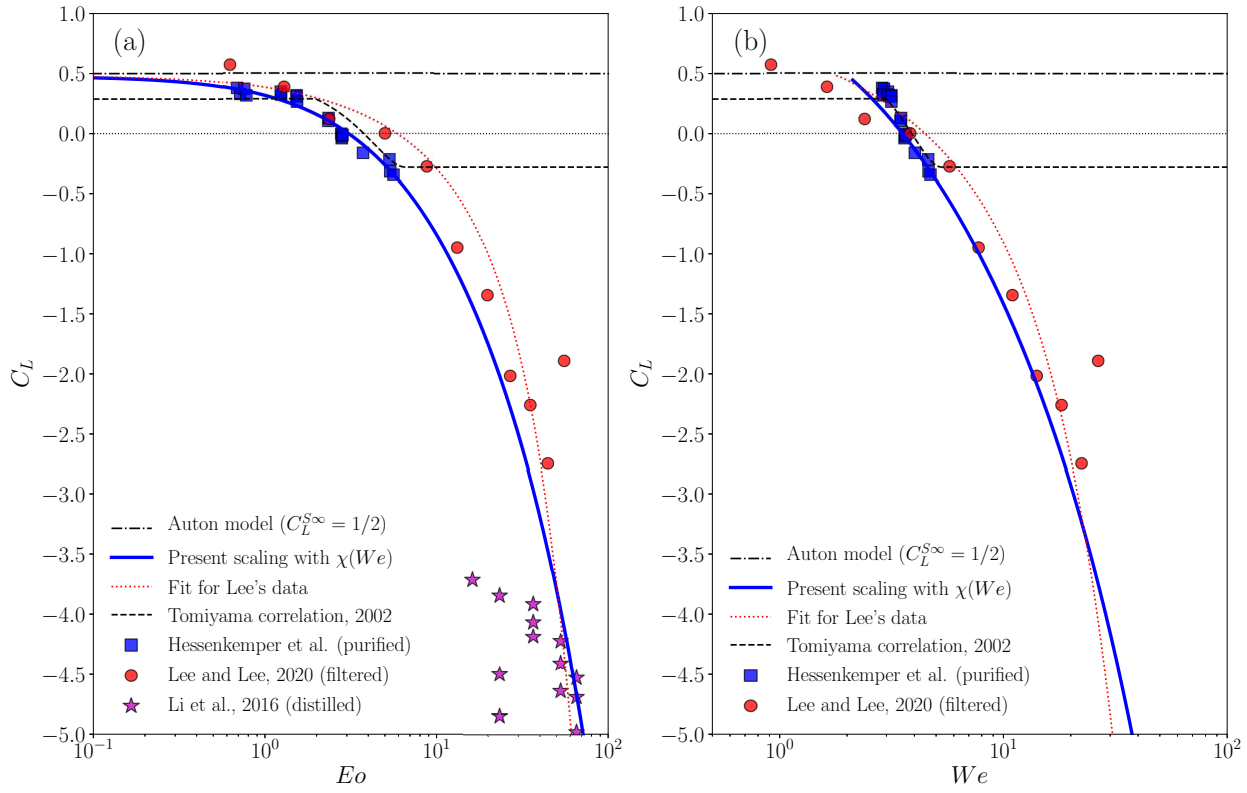

Figure 9: Lift coefficient data in comparison with the present scaling, Eq. (35), in which Eqs. (19) and (24) are used to calculate Re and χ, respectively. (a) C_L-Eo plane, (b) C_L-We plane.

proposed by Tomiyama et al. (2002b) is also drawn in the figure:

$$C_L = \begin{cases} \min[0.288\tanh(0.121Re), f_T(Eo_H)] & \text{for } Eo_H < 4 \\ f_T(Eo_H) & \text{for } 4 \le Eo_H \le 10.7 \end{cases} \tag{36}$$

$$f_T(Eo_H) = 0.00105Eo_H^3 - 0.0159Eo_H^2 - 0.0204Eo_H + 0.474 \tag{37}$$

The constants, $a = 0.94$ and $b = 0.0875$, in Eq. (20) obtained for Hessenkemper's data were used for the shape correlation to draw the lift curve. Though this correlation was developed for bubbles in the μ regime, it reasonably agrees with Hessenkemper's data and the critical Eo for the lift reversal is also close to the data. This might be why Tomiyama's correlation has given reasonable predictions of bubbly flows in low viscosity systems, e.g. Lucas and Tomiyama (2011).

The dotted line in the figure represents Eq. (35), for which χ was evaluated using a function $\chi(We)$ fitted to Lee's data (see Appendix B). Good agreement between Eq. (35) and the data implies that the functional form of the present scaling is valid not only for the clean system but also for the contaminated system. The derivation of Eq. (35) for the contaminated system is given in Appendix B. Experimental data of Li et al. (2016a) are also plotted in the figure. Note that they are shown just for reference because there are some uncertainty in the data: (1) distilled water used in their experiments were not clean due to unexpected contamination by a capillary tube for bubble generation and/or seeding particles for velocimetry (Li et al., 2016b; Lee and Lee, 2020), and (2) information on the relevant dimensionless groups, e.g. χ, were provided for some limited cases. Though the data largely scatter and the dependence on Eo is not clear, C_L at large Eo are on the C_L curve of Eq. (35) and the curves for Hessenkemper's data and Lee's data are close with each other at that large Eo range. It can therefore be speculated that the influence of contamination on C_L of deformed bubbles becomes weak as Eo increases, i.e. deformation increases.

Figure 9(b) shows the C_L data plotted against We. Note that applying the force balance, $C_D = 4/3Fr^2$, to the relation, $We = Fr^2Eo$, yields $We = 4Eo/3C_D$. Hence the data points were just shifted horizontally by C_D when converting the horizontal axis from Eo to We. The present scaling works well for both datasets on the C_L-We plane.

4.3. Summary of Relations between C_L and C_D

The discussion on C_D in the air-water systems revealed that the negative lift governed by the vorticity produced at the bubble surface is tightly connected with the drag. The connection between the drag and the lift acting on a clean bubble can be summarized as follows.

For spherical bubbles in the Stokes regime, Legendre and Magnaudet (1997) derived the following relation between the lift and drag coefficients: $C_L^S = (3J(\varepsilon)/8\pi^2\varepsilon)C_D$, where ε is the dimensionless number defined by $\varepsilon = (Sr/Re)^{1/2}$ and $J(\varepsilon)$ the value of a three-dimensional integral: $J(\infty) = 2.255$ (McLaughlin, 1991). The drag coefficient is given by the Hadamard-Rybczynski solution, i.e. $C_D = 16/Re = 16\omega^*_{\max}/Re$, where $\omega^*_{\max} = 1$ for

Table 2: List of correlations for evaluating C_L in air-water system. C_L^S is given by the correlation of Legendre and Magnaudet (1998). The functions and the coefficients are as follows: $\gamma_e = 0.048$, $g(M) = a\exp(-bM^c)$, $h(M) = p\exp(-qM^r)$, $a = 500$, $b = 6.0$, $c = 0.0735$, $p = 3.46$, $q = 5.4$, $r = 0.191$.

μ regime	σ-i regime
$C_D = \frac{16}{Re}\left(1 + 0.25\chi^{1.9}Re^{0.32}\right)$	$C_D = \frac{8}{3}\frac{Eo}{Eo+4}$
$C_L = C_L^S - \frac{g(M)(\chi-1)^{h(M)}}{Re}$	$C_L = C_L^S - \gamma_e\omega_{\max}^{*\infty}\left[\frac{8Eo}{3(Eo+16(\chi^2-1)/\chi^{8/3})}\right]$
$\chi = \left[1 + 0.016Eo^{1.12}Re\right]^{0.388}$	$\chi = 1 + 0.62We^{0.376}$

spherical bubbles in the Stokes regime (Legendre, 2007). Legendre and Magnaudet (1998) obtained the empirical correlation, $C_L^S = C_L^{S\infty}(1+16/Re)/(1+29/Re)$, for spherical bubbles of high Reynolds numbers. This correlation can be approximated as $C_L^S = C_L^{S\infty} - 6.5/Re$ at high Re. Hence the viscous contribution in the second term is obviously negative and proportional to the drag coefficient, $C_D = 48/Re = 16\omega_{\max}^*/Re$, where $\omega_{\max}^* = 3$ (Levich, 1962; Legendre, 2007). Note that $C_L^{S\infty} = 1/2$ for spherical bubbles in an inviscid liquid does not have any relation with C_D (in other words no correction term in terms of C_D appears in $C_L^{S\infty}$) since the drag vanishes in the potential flow.

For ellipsoidal bubbles in the μ regime, we (Hayashi et al., 2020) showed by using Aoyama's data that the negative lift is connected with ω as pointed out by Adoua et al. (2009) and the decay of the lift also follows the behavior of Re^{-1} as is the case with the drag. The lift reversal can therefore be expressed in the form of $C_L = C_L^{S\infty} - G_r(\chi, Re)C_D(\chi, Re)$, and, by making use of the maximum vorticity, $\omega_{\max}^{*\infty}$, (Magnaudet and Mougin, 2007) and the deformation-inertia factor, $\phi(\chi, Re)$ $(= 0.25\chi^{1.9}Re^{0.32})$, in C_D, we obtained $C_L = C_L^{S\infty} - (16/Re)[\gamma_r\omega_{\max}^{*\infty}(\chi)\phi(\chi, Re)]$, where $\gamma_r = 0.078$. In the present study, we obtained a similar relation for the lift reversal in the σ-i regime, i.e. $C_L = C_L^{S\infty} - G_e(\chi, Eo)C_D(\chi, Eo)$, and the empirical equation was obtained as $C_L = C_L^{S\infty} - \gamma_e\omega_{\max}^{*\infty}(8Eo/3(Eo + 16(\chi^2 - 1)/\chi^{8/3}))$, where $\gamma_e = 0.048$.

The bubble Reynolds number, the aspect ratio, the drag coefficient and the lift coefficient in the air-water system in the μ and σ-i regimes are calculated as shown in Fig. 10 and the correlations used in the calculation are given in Table 2, where the shape correlation for the

μ regime

$$\chi = (1 + 0.016Eo^{1.12}Re)^{0.388} \tag{38}$$

was proposed by Aoyama et al. (2016), whose applicable range is $-11 \leq \log M \leq 0.63$, and the drag correlation

$$C_D = \frac{16}{Re}\left[1 + \phi(\chi, Re)\right] \tag{39}$$

was proposed by Chen et al. (2019). The transition between the μ regime and the σ-i regime was determined as an intersection of the drag curves in these regimes and, at $\log M = -10.58$, the intersection appears at $(Eo, Re) = (2.56, 460)$. It can be seen that the correlations can give good evaluations of C_D and C_L in both regimes. The shape correlations have a gap in χ at the regime transition. However the effect of the gap on C_L is negligible from a practical point of view. The following expression can be used instead of the transition, $Eo = 2.56$, to avoid the gap as shown by the dotted line in the figure:

$$\chi = \min\left[\chi_r(We), \chi_e(We)\right] \tag{40}$$

where χ_r and χ_e are given by Eqs. (23) and (24), respectively. The transition for the χ equation is at $We \approx 3.12$.

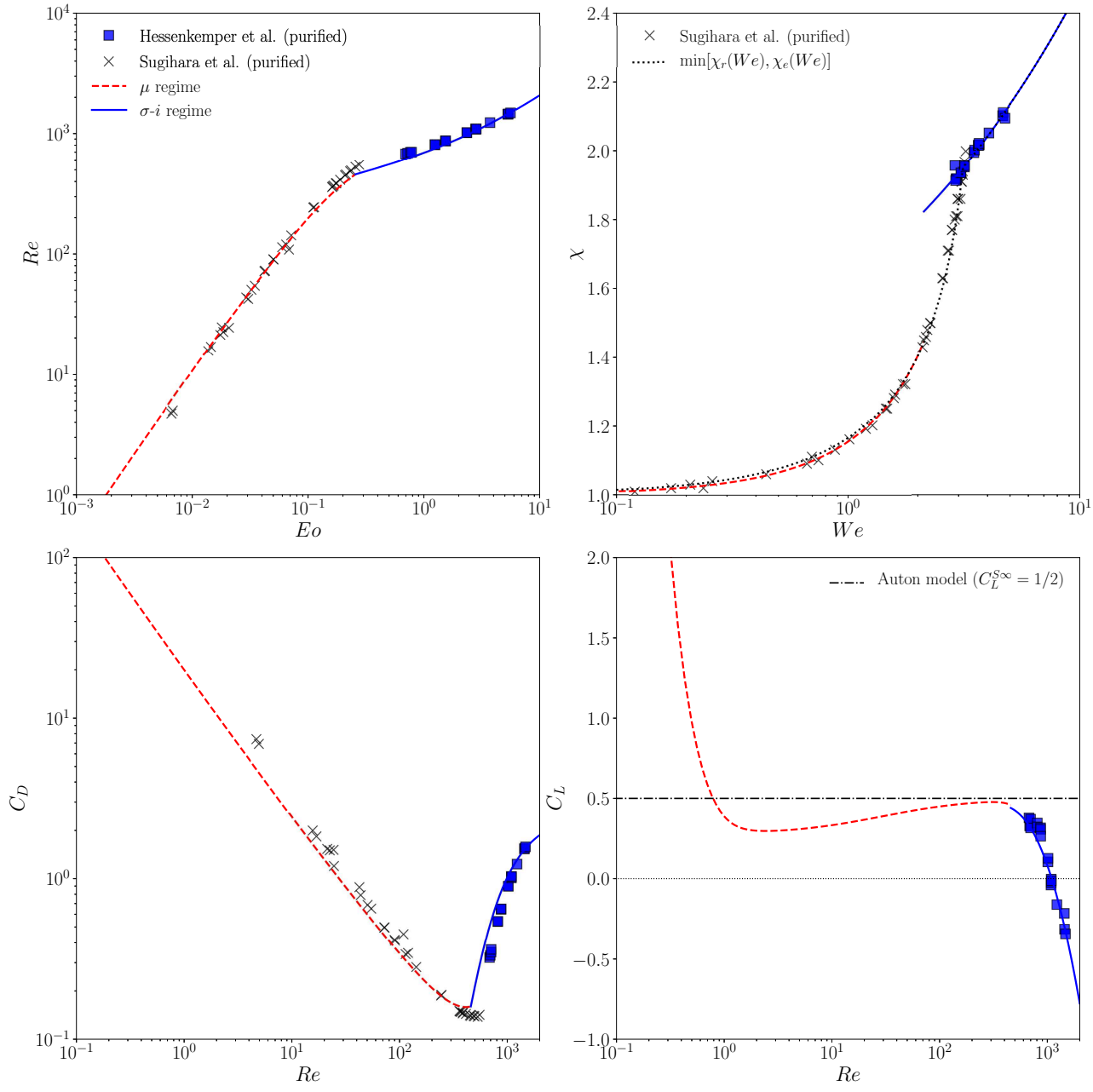

Figure 10: Bubble Reynolds number, aspect ratio, drag coefficient and lift coefficient in air-water system calculated using empirical correlations tabulated in Table 2. The transition between the μ regime and the σ-i regime appears at $(Eo, Re) = (2.56, 460)$ for $M = 2.6 \times 10^{-11}$.

5. Conclusion

In this study we discussed scaling of the lift coefficient of a deformed bubble in the surface tension-inertial force dominant regime. For this purpose we made use of the lift databases of Hessenkemper et al. (2021) and Lee and Lee (2020) for bubbles in air-water systems. We first made a brief data analysis and confirmed that the former and latter data are for pure and contaminated systems, respectively. We then made it clear that the lift reversal of clean bubbles in the σ-i regime is connected to the drag via the vorticity produced at the bubble surface as in the viscous force dominant regime (Hayashi et al., 2020), and a simple scaling, which gives good evaluations of C_L, was presented. In addition, the proposed scaling was confirmed to be applicable to C_L of contaminated bubbles.

Acknowledgement

A. Tomiyama and K. Hayashi would like to express their thanks to financial supports by JSPS KAKENHI, Grant No. 18H03756 and 20K04267.

Appendix A. Turbulence effect on C_D and C_L

Kojima et al. (1975) carried out experiments on single bubbles suspended stationary by a downward liquid flow. They showed that the drag coefficient in a liquid flow of $I = 0.13$ in the σ-i regime ($2000 < Re < 5000$) was almost the same as that in an undisturbed flow, where I is the turbulence intensity of a liquid flow. Merle et al. (2005) also showed in their large-eddy simulations of a single spherical bubble in a turbulent pipe flow that the presence of turbulence did not affect C_D when $I \ll 1$. The I in Lee's experiment were smaller than 0.1 and they confirmed that C_D in the linear shear flow with the weak turbulence were the same as those in stagnant water. Merle et al. (2005) also pointed out that Auton's lift model gave an accurate evaluation of the transverse force of a spherical bubble in weak turbulence ($I = 0.064$), even though the bubble size was comparable with the Taylor microscale. According to Merle's results, it can be speculated that the presence of the weak turbulence in Lee's experiment does not affect C_L.

The effects of weak turbulence have thus been confirmed small, and therefore, the present scaling of C_L is expected to be applicable to deformed bubbles under weak turbulence. It should however be noted that a strong turbulence may affect both C_D and C_L. Recently Salibindla et al. (2020) experimentally investigated the drag and lift acting on single deformed bubbles in a strong liquid turbulence, i.e. the fluctuation velocity was 0.25 m/s, which is comparable to the typical rise velocity of millimeter bubbles. The C_D were confirmed to decrease by turbulence at Re larger than 400 (in the σ-i regime). They also pointed out that a strong turbulence enhances shape deformation, causing decrease in C_L and the critical bubble diameter for lift reversal. Under the strong turbulence, C_L is governed by the turbulence-based Weber number, We_ϵ, controlling the turbulence-induced bubble deformation and the lift reversal takes place between $We_\epsilon = 0.71$ and 1 (between $d = 2.2$ and 2.7 mm in the air-water system).

Appendix B. Fitting to Lee's data

Although Lee's data must be for contaminated bubbles, it is worth examining the applicability of the present scaling, Eq. (35), to them. Let us first express the C_D data in terms of χ and Eo. The following equation fits the data for the wide range of Eo in Lee's data as shown in Fig. B.1:

$$g_e(\chi) = 0.65/\chi^{2.7} \tag{B.1}$$

The curve is drawn by using their shape correlation, $\chi = 1 + 0.21Eo^{0.58}$. By assuming the functional form, Eq. (35), evaluating the product, $G_e g_e$, for Lee's data gives values shown in Fig. B.2. They are approximately constant even for the wide range of Eo and close to that for the clean system, i.e. $\gamma_e = 0.048$. Hence the functional form of Eq. (35) is common for the clean system of Hessenkemper et al. (2021) and the contaminated system of Lee and Lee (2020) and the difference appears only in the shape correlation. This implies that shape is a key factor for C_D and C_L in the σ-i regime. Being similar to Hessenkemper's data, the aspect ratio in Lee's data can also be correlated in terms of We:

$$\chi = 1 + 0.23We^{0.69} \tag{B.2}$$

A comparison between the present scaling with the data of the contaminated system is shown in Fig. 9, showing very good agreement. Here Eq. (B.2) was used for χ. The value of γ_e can be slightly increased to obtain better evaluations around $C_L = 0$ if needed.

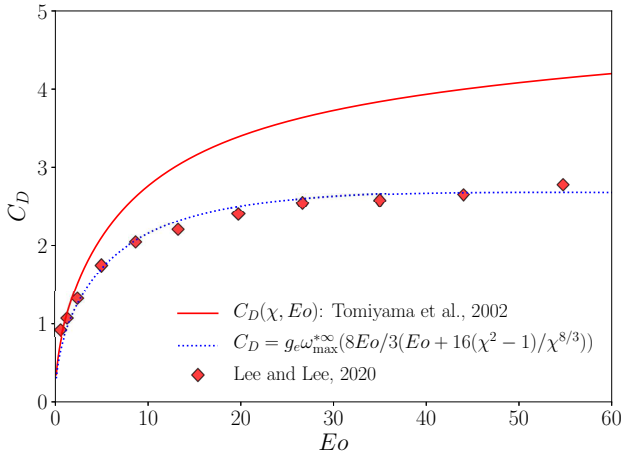

Figure B.1: C_D data compared with $C_D(\chi, Eo)$ (Tomiyama et al., 2002a).

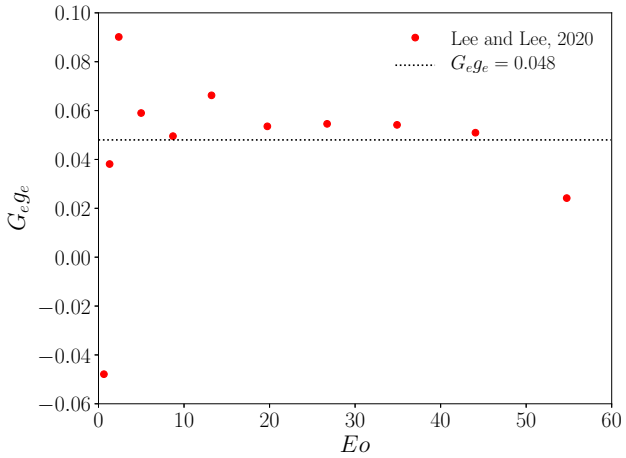

Figure B.2: Product of the factor $G_e(\chi, Eo)g_e(\chi)$ in contaminated case.

References

Adoua, R., Legendre, D., Magnaudet, J., 2009. Reversal of the lift force on an oblate bubble in a weakly viscous linear shear flow. Journal of Fluid Mechanics 628, 23–41.

Aoyama, S., Hayashi, K., Hosokawa, S., Lucas, D., Tomiyama, A., 2017. Lift force acting on single bubbles in linear shear flows. International Journal of Multiphase Flow 96, 113–122.

Aoyama, S., Hayashi, K., Hosokawa, S., Tomiyama, A., 2016. Shapes of ellipsoidal bubbles in infinite stagnant liquids. International Journal of Multiphase Flow 79, 23–30.

Auton, T. R., 1987. The lift force on a spherical body in a rotational flow. Journal of Fluid Mechanics 183, 199–218.

Aybers, N. M., Tapucu, A., 1969. Studies on the drag and shape of gas bubbles rising through a stagnant liquid. Wärme- und Stoffübertragung 2, 171–177.

Chen, J., Hayashi, K., Hosokawa, S., Tomiyama, A., 2019. Drag correlations of ellipsoidal bubbles in clean and fully-contaminated systems. Multiphase Science and Technology 31(3), 215–234.

Clift, R., Grace, J., Weber, M., 1978. Bubbles, Drops, and Particles. Academic Press.

de Vries, A., Biesheuvel, A., van Wijngaarden, L., 2002. Notes on the path and wake of a gas bubble rising in pure water. International Journal of Multiphase Flow 28(11), 1823–1835.

Duineveld, P. C., 1995. The rise velocity and shape of bubbles in pure water at high Reynolds number. Journal of Fluid Mechanics 292, 325–332.

Ervin, E., Tryggvason, G., 1997. The rise of bubbles in a vertical shear flow. Journal of Fluids Engineering 119, 443–448.

Fan, L.-S., Tsuchiya, K., 1990. Bubble Wake Dynamics in Liquids and Liquid–Solid Suspensions. Butterworth-Heinemann.

Hayashi, K., Legendre, D., Tomiyama, A., 2020. Lift coefficients of clean ellipsoidal bubbles in linear shear flows. International Journal of Multiphase Flow 129, 103350.

Hessenkemper, H., Ziegenhein, T., Lucas, D., 2020. Contamination effects on the lift force of ellipsoidal air bubbles rising in saline water solutions. Chemical Engineering Journal.

Hessenkemper, H., Zieghenein, T., Rzehak, R., Lucas, D., Tomiyama, A., 2021. Lift force coefficient of ellipsoidal single bubbles in water. International Journal of Multiphase Flow 138, 103587.

Kariyasaki, A., 1987. Behavior of a gas bubble in a liquid velocity profile. Transactions of Japan Society of Mechanical Engineers, Series B (in Japanese) 53, 744–749.

Kojima, E., Akehata, T., Shirai, T., 1975. Behavior of single air bubbles held stationary in downward flows. Journal of Chemical Engineering of Japan 8(2), 108–113.

Lee, W., Lee, J.-Y., 2020. Experiment and modeling of lift force acting on single high Reynolds number bubbles rising in linear shear flow. Experimental Thermal and Fluids Science 115, 110085.

Legendre, D., 2007. On the relation between the drag and the vorticity produced on a clean bubble. Physics of Fluids 19, 018102.

Legendre, D., Magnaudet, J., 1997. A note on the lift force on a spherical bubble or drop in a low-Reynolds-

number shear flow. Physics of Fluids 9, 3572–3574.

Legendre, D., Magnaudet, J., 1998. The lift force on a spherical bubble in a viscous linear shear flow. Journal of Fluid Mechanics 368, 81–126.

Legendre, D., Zenit, R., Velez-Cordero, J. R., 2012. On the deformation of gas bubbles in liquids. Physics of Fluids 24(4), 043303.

Levich, V., 1962. Physicochemical Hydrodynamics. Prentice Hall.

Li, Z., Song, X., Jiang, S., Ishii, M., 2016a. The lateral migration of relative large bubble in simple shear flow in water. Experimental Thermal and Fluid Science 77, 144–158.

Li, Z., Zhao, Y., Song, X., Yu, H., Jiang, S., Ishii, M., 2016b. Experimental investigation of single small bubble motion in linear shear flow in water. Nuclear Engineering and Design 305, 334–346.

Lucas, D., Tomiyama, A., 2011. On the role of the lateral lift force in poly-dispersed bubbly flows. International Journal of Multiphase Flow 37, 1178–1190.

Lunde, K., Perkins, R., 1998. Shape oscillations of rising bubbles. Applied Scientific Research 58, 387–408.

Magnaudet, J., Mougin, G., 2007. Wake instability of a fixed spheroidal bubble. Journal of Fluid Mechanics 572, 311–337.

McLaughlin, J. B., 1991. Inertial migration of a small sphere in linear shear flows. Journal of Fluid Mechanics 224, 261–274.

Merle, A., Legendre, D., Magnaudet, J., 2005. Forces on a high-Reynolds-number spherical bubble in a turbulent flow. Journal of Fluid Mechanics 532, 53–62.

Saffman, P., 1992. Vortex Dynamics. Cambridge University Press.

Salibindla, Ashwanth, K. R., Mohammad Masuk, A. U., Tan, S., Ni, R., 2020. Lift and drag coefficients of deformable bubbles in intense turbulence determined from bubble rise velocity. Journal of Fluid Mechanics 894, A20.

Sugihara, K., Sanada, T., Shirota, M., Watanabe, M., 2007. Behavior of single rising bubbles in superpurified water. Kagaku-Kogaku Ronbunshu (in Japanese) 33, 402–408.

Tomiyama, A., 1998. Struggle with computational bubble dynamics. Multiphase Science and Technology 10, 369–405.

Tomiyama, A., Celata, G., Hosokawa, S., Yoshida, S., 2002a. Terminal velocity of single bubbles in surface tension force dominant regime. International Journal of Multiphase Flow 28, 1497–1519.

Tomiyama, A., Kataoka, I., Zun, I., Sakaguchi, T., 1998. Drag coefficients of single bubbles under normal and micro gravity conditions. JSME International Journal Ser. B: Fluids and Thermal Engineering 41(2), 472–479.

Tomiyama, A., Tamai, H., Žun, I., Hosokawa, S., 2002b. Transverse migration of single bubbles in simple shear flows. Chemical Engineering Science 57, 1849–1858.

Veldhuis, C., Biesheuvel, A., van Wijngaarden, L., 2008. Shape oscillations on bubbles rising in clean and in tap water. Physics of Fluids 20, 2911042.

Wellek, R. M., Agrawal, A. K., Skelland, A. H. P., 1966. Shapes of liquid drops moving in liquid media. A.I.Ch.E. Journal 12, 854–862.

Ziegenhein, T., Tomiyama, A., Lucas, D., 2018. A new measuring concept to determine the lift force for distorted bubbles in low Morton number system: Results for air/water. International Journal of Multiphase Flow 108, 11–24.